THE ROYAL SOCIETY

Published online 4 October 2002

Structure of the manganese complex in photosystem II: insights from X-ray spectroscopy

Vittal K. Yachandra

Melvin Calvin Laboratory, Physical Biosciences Division, Lawrence Berkeley National Laboratory, Berkeley, CA 94720, USA

We have used Mn K-edge absorption and Kβ emission spectroscopy to determine the oxidation states of the Mn complex in the various S states. We have started exploring the new technique of resonant inelastic X-ray scattering spectroscopy; this technique can be characterized as a Raman process that uses K-edge energies (1s to 4p, *ca.* 6550 eV) to obtain L-edge-like spectra (2p to 3d, *ca.* 650 eV). The relevance of these data to the oxidation states and structure of the Mn complex is presented. We have obtained extended X-ray absorption fine structure data from the S_0 and S_3 states and observed heterogeneity in the Mn–Mn distances leading us to conclude that there may be three rather than two di-μ-oxo-bridged units present per tetranuclear Mn cluster. In addition, we have obtained data using Ca and Sr X-ray spectroscopy that provide evidence for a heteronuclear Mn–Ca cluster. The possibility of three di-μ-oxo-bridged Mn–Mn moieties and the proximity of Ca is incorporated into developing structural models for the Mn cluster. The involvement of bridging and terminal O ligands of Mn in the mechanism of oxygen evolution is discussed in the context of our X-ray spectroscopy results.

Keywords: extended X-ray absorption fine structure; oxygen-evolving complex; photosystem II; X-ray absorption near-edge structure; X-ray absorption spectroscopy; X-ray emission spectroscopy

1. INTRODUCTION

There are two critical questions related to the process of photosynthetic water oxidation catalysed by a Mn cluster in the OEC of PSII. These questions are as follows.

(i) What are the oxidation state(s) and structural changes in the Mn complex as the OEC proceeds through the S-state cycle?
(ii) What is the mechanism by which four electrons are removed from two water molecules by the Mn complex to produce an O_2 molecule?

We have addressed these questions principally by the use of XANES, Kβ XES and EXAFS along with electron paramagnetic resonance spectroscopy (Yachandra *et al.* 1996; Robblee *et al.* 2001).

X-ray spectroscopy is element specific and can monitor Mn (or Ca or Sr) directly in the membrane; hence, it is a good method for studying the structure of the Mn OEC without interference from pigment molecules, the lipid and protein matrix, or other metals such as Ca, Mg, Cu or Fe that are present in active PSII preparations. Mn K-edge XANES and Kβ XES provide information about oxidation states and the site symmetry of the Mn complex, and EXAFS at the Mn or Sr or Ca K edge furnishes information about the number, type and distances to neighbouring ligand atoms in the S_0, S_1, S_2 and S_3 states of the OEC (Yachandra 1995; Yachandra & Klein 1996). X-ray spectroscopy does not require long-range order; the structural studies can be performed on frozen solutions. Several of the intermediate states mentioned above can be stabilized as frozen solutions. Few other spectroscopic techniques provide such specificity for studying the structure of Mn in the OEC.

This paper focuses on the application of X-ray spectroscopic methods to resolve structural questions regarding the Mn cluster in the OEC and we present our view of the structure of the Mn cluster that is refined based on new data, and a mechanism for water oxidation that emphasizes the recent results from our laboratory.

2. OXIDATION STATES OF THE MANGANESE CLUSTER

A key question for the understanding of photosynthetic water oxidation is whether the four oxidizing equivalents generated by the reaction centre are accumulated on the four Mn ions of the OEC during S-state turnover, or whether a ligand-centred oxidation takes place, especially, before the formation and release of molecular oxygen during the S_3 to S_4 to S_0 transition. We have addressed these questions by using Mn K-edge XANES (1s to 4p absorption), Kβ XES (3p to 1s emission) and the recently introduced RIXS (1s to 3d or 4p absorption followed by 2p to 1s Kβ emission) to obtain L-edge-like spectra (2p to 3d absorption).

A promising approach to studying the Mn oxidation states in the native S states is to step samples through the S-state cycle by the application of saturating single-turn-

One contribution of 21 to a Discussion Meeting Issue 'Photosystem II: molecular structure and function'.

over flashes and to characterize these samples by X-ray spectroscopy. We reported earlier XANES data from samples in the S_0 through S_3 states produced under these physiologically relevant conditions (Roelofs *et al.* 1996). The flash-advanced PSII samples prepared from spinach exhibited XANES spectra that showed Mn oxidation from S_0 to S_1 and from S_1 to S_2, but no further oxidation during the S_2 to S_3 transition. These results are consistent with our earlier studies by Guiles *et al.* (1990*a*,*b*) that were prepared by illumination at low temperature or by chemical treatment.

Other spectroscopic techniques such as NMR–PRE (Sharp 1992), EPR (Dismukes & Siderer 1981; Hansson & Andréasson 1982; Ahrling *et al.* 1997; Messinger *et al.* 1997*b*), UV absorption (Dekker 1992; Van Leeuwen *et al.* 1993) and Y_D^{ox} EPR–spin echo (Styring & Rutherford 1988) studies show that, in PSII, the S_0 to S_1 and S_1 to S_2 transitions are Mn-centred oxidations, and most groups agree that Mn redox states in the S_1 state are (III_2, IV_2) that are oxidized to (III, IV_3) in the S_2 state. There is, however, a long-standing controversy as to whether a Mn- or ligand-centred oxidation occurs in the S_2 to S_3 transition (Ono *et al.* 1992; Iuzzolino *et al.* 1998).

To resolve the controversy we used high-resolution Mn Kβ X-ray fluorescence studies in collaboration with Steve Cramer, who has constructed a unique high-resolution emission spectrometer that operates at the Mn Kβ fluorescence energy and has demonstrated the feasibility of determining the oxidation states of Mn (Bergmann & Cramer 1998). We have completed a comprehensive Mn Kβ XES study in conjunction with XANES on sets of samples prepared in a similar manner and characterized by EPR (Messinger *et al.* 2001).

Due to the fact that the actual S-state composition is of critical importance to the interpretation of the results, we characterized the samples by EPR spectroscopy, using the S_2 multiline EPR signal as a direct measure for the amount of S_2 in our samples (figure 1). The relative S-state populations in samples given none, one, two, three, four, five or six flashes were determined from fitting the flash-induced EPR multiline signal oscillation pattern to the model of Kok *et al.* (1970) for each of the samples used in the X-ray spectroscopy experiments. It is essential to obtain high concentrations of PSII in the S states to obtain EPR, XANES and Kβ spectroscopy data with a good signal-to-noise ratio. An Nd-YAG laser system (Spectra-Physics PRO 230-10, 800 mJ pulse^{-1} at 532 nm, 9 ns pulse width) was used to illuminate PSII samples from both sides simultaneously. Due to the fact that the pulse widths are narrow compared with those of a flash lamp, double hits become negligible. The damping of the oscillation pattern is minimized, thus making it possible to derive an unique set of spectra by deconvolution. When the system becomes scrambled by frequent misses and double hits, the deconvolved spectra are not unique.

(a) *Manganese K-edge X-ray absorption near-edge structure*

Our edge data are of sufficient signal-to-noise quality to allow for not only a determination of the absorption edge position (using the inflection point energy, defined as the zero-crossing in the second derivative of the edge), but also an analysis of the structure on the edge as a function of the number of flashes.

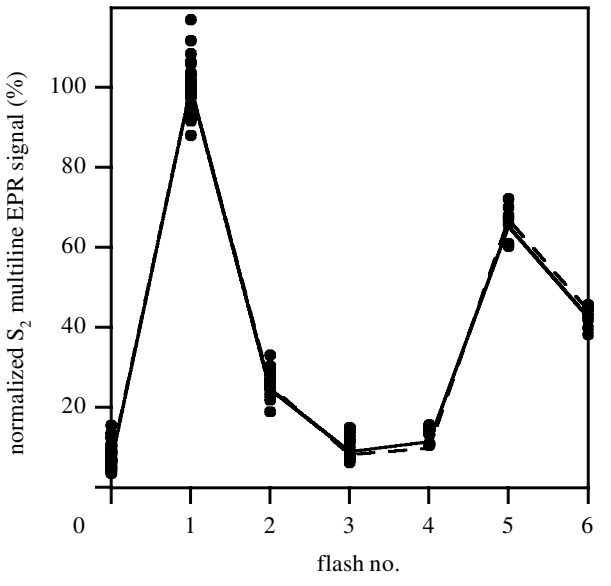

Figure 1. The S_2 multiline EPR signal amplitudes are shown as a function of flash number (solid line, experimental average). The best fit to the S_2 multiline oscillation pattern is shown as a dashed line (simulation). The S-state compositions of the samples are derived from the fit. Individual S-state spectra can be uniquely determined from these data if the oscillation pattern is as pronounced as shown in the figure. It is important that a deep oscillation pattern is obtained, because all subsequent steps that are used in the deconvolution to generate pure S-state spectra are critically dependent on these data.

The edge spectra of samples given none, one, two, or three flashes are combined with EPR information to calculate the pure S-state edge spectra. The shifts in inflection point energy positions and changes in shape are determined by second derivatives of the K-edge spectra and are shown in figure 2. In addition to the shift in edge position, the S_0 to S_1 (2.1 eV) and S_1 to S_2 (1.1 eV) transitions are accompanied by characteristic changes in the shape of the edge, also indicative of Mn oxidation. The edge position shifts very little (0.3 eV) for the S_2 to S_3 transition, and the edge shape shows only minor changes (Messinger *et al.* 2001).

(b) *Kβ X-ray emission spectroscopy*

High-resolution Mn XES was performed on S_0, S_1, S_2 and S_3 samples prepared using high-power laser flashes as described above. In this technique, the energy of the Mn Kβ emission (3p to 1s) is measured with a high-resolution dispersive spectrometer. The shape and energy of the $K\beta_{1,3}$ emission reflect the oxidation state(s) of the emitting Mn atom(s). The emission occurs from a 3p level that is mainly influenced by the number of unpaired 3d electrons, and it is less sensitive to the symmetry and bonding than the K-edge absorption, which involves transitions to the 4p level (Peng *et al.* 1994). The spin of the unpaired 3d valence electrons can be either parallel (Kβ′) or antiparallel ($K\beta_{1,3}$) to the hole in the 3p level. The splitting between the Kβ′ and $K\beta_{1,3}$ peaks becomes smaller for higher oxidation states because fewer 3d electrons interact with the 3p hole. Thus, in contrast to the inflection points

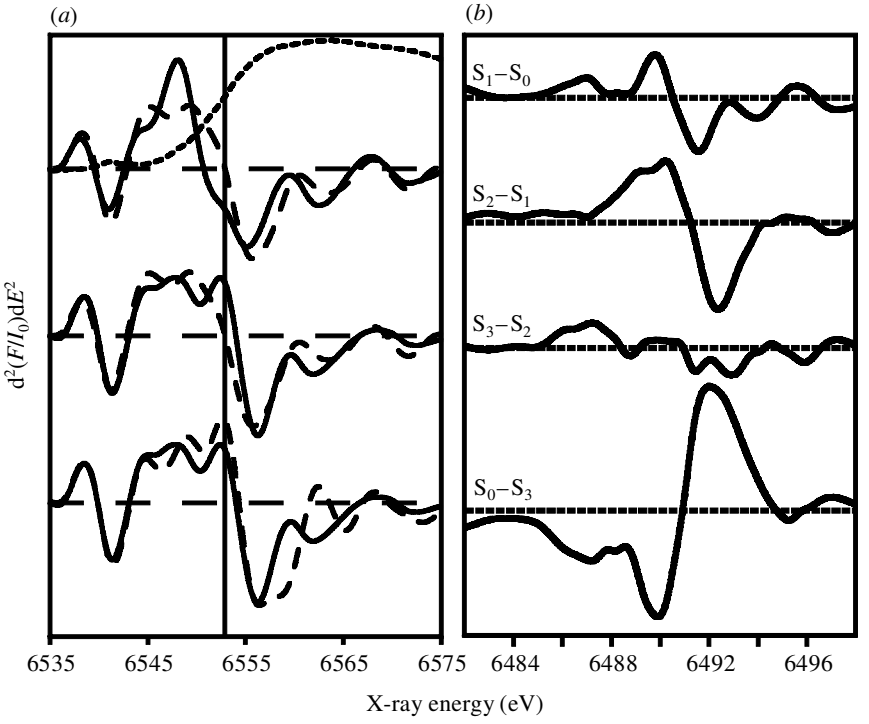

Figure 2. (*a*) Second derivatives of the normalized pure S-state Mn K-edge spectra of the Mn cluster of PSII. For clarity a vertical line has been drawn at the inflection-point energy of the S_1 state. The states are as follows: top—solid line, S_0, dashed line, S_1; middle—solid line, S_2, dashed line, S_1; bottom—solid line, S_2, dashed line, S_3. The change in IPE (△ in eV) for each S-state advance is as follows: top, 2.1 eV; middle, 1.1 eV; bottom, 0.3 eV . For reference, the K-edge spectrum of the S_1 state is also plotted (dotted line). (*b*) The S_1-S_0, S_2-S_1, S_3-S_2 and S_0-S_3 difference high-resolution Mn X-ray Kβ-emission spectra. The derivative shapes indicate shifts in the energy of the spectra between the S_0 and S_1, and S_1 and S_2 spectra, indicating oxidations of Mn. The S_3-S_2 difference spectra demonstrates the similarity of the spectra, indicating that this advance does not involve an Mn-centred oxidation.

of the XANES edges, the $K\beta_{1,3}$ peaks shift to a lower energy with higher oxidation states.

Using a first-moment analysis, the position of the main $K\beta_{1,3}$ peak has been calculated for each S state. Based on the shifts, or lack thereof, of the first moments, we concluded that Mn is not oxidized during the $S_2 \rightarrow S_3$ transition. Our results (shown as difference spectra in figure 2) show a shift in energy between the S_0- and S_1-state spectra and between the S_1- and S_2-state spectra and seen in the derivative-shaped difference spectra. However, there is very little change between the S_2 and S_3 states, as seen in the difference spectrum (Messinger *et al.* 2001).

We have used two independent spectroscopic techniques, Kβ and XANES spectroscopy, along with EPR, to examine the Mn redox states in PSII. Figure 3 summarizes the oscillation patterns of the first moments from the $K\beta_{1,3}$ spectra and of the XANES spectra inflection point energies. Both patterns show large shifts between the 0F and 1F samples, which reflect the Mn-centred oxidation during the $S_1 \rightarrow S_2$ transition. A much smaller shift occurs between the 1F and 2F samples, which is inconsistent with a Mn-centred oxidation during the $S_2 \rightarrow S_3$ transition. The second derivatives of the S-state XANES spectra and the Kβ difference spectra (figure 2) confirm this conclusion. It is unlikely that both techniques would fail to detect a Mn-centred oxidation for the $S_2 \rightarrow S_3$ transition if it did, in fact, occur. Support for this conclusion has also come from XANES and Kβ studies of two sets of structurally homologous Mn compounds in different oxidation states (Visser *et al.* 2001). We conclude that probably no direct Mn oxidation is involved in this transition. The proposed Mn-oxidation state assignments are as follows: S_0 (II, III, IV, IV) or (III, III, III, IV); S_1 (III, III, IV, IV); S_2 (III, IV, IV, IV); S_3 (III, IV, IV, IV) (Messinger *et al.* 2001).

(c) *Resonant inelastic X-ray scattering spectroscopy*

Mn L-edge spectra have several advantages over Mn K-edge spectra, because multiplet calculations can be applied to L-edge spectra that are sensitive to the number of holes in the 3d level, the oxidation state of Mn, and the spin state of Mn. This is a rich amount of information about oxidation states relative to what is available from K-edge XANES spectra. L-edge spectra have already been obtained for a number of Fe, Cu and Ni metalloproteins, and have been simulated using multiplet calculations to provide quantitative conclusions about the oxidation states of the metals involved (Wang *et al.* 1996, 1997). However, the main disadvantage of using soft X-rays, where the Mn L-edge occurs (*ca.* 650 eV), is that the samples are subjected to ultra-high vacuum and are more prone to X-ray damage.

We have recently started exploring the RIXS technique that circumvents the problems mentioned above in a very elegant manner. It is possible to combine the two types of K- and L-edge experiments by mapping the 1s2p RIXS landscape as shown in figure 4 in a simplified two-step process (Caliebe *et al.* 1998). RIXS involves exciting a pre-edge transition (1s to 3d) of the K shell using hard X-

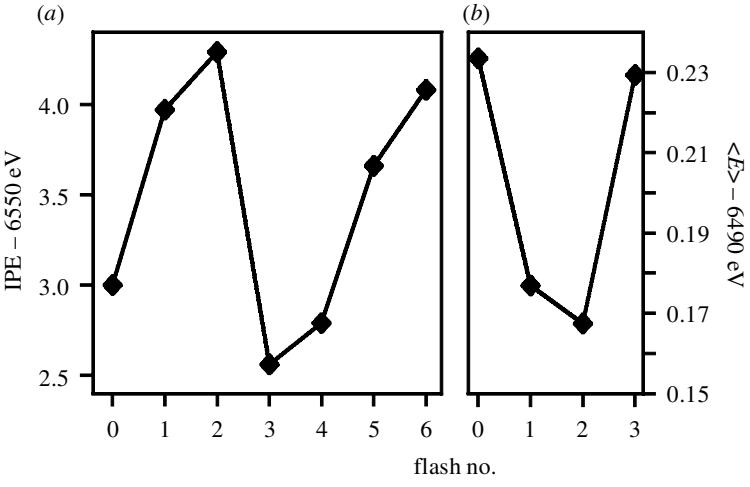

Figure 3. (*a*) IPE (in eV) of the Mn K-edge of PSII membranes as a function of the number of applied flashes. (*b*) The first moments of the Mn Kβ fluorescence spectra (<*E*>) as a function of flash number. The Mn K-edge shifts to higher energy as Mn is oxidized. The first moment of the Mn Kβ fluorescence shifts to lower energy as Mn is oxidized. The complementary and mutually reinforcing results provide a strong case for Mn oxidation during the S_0 to S_1 and S_1 and S_2 advances but no Mn-centred oxidation at the S_2 to S_3 advance.

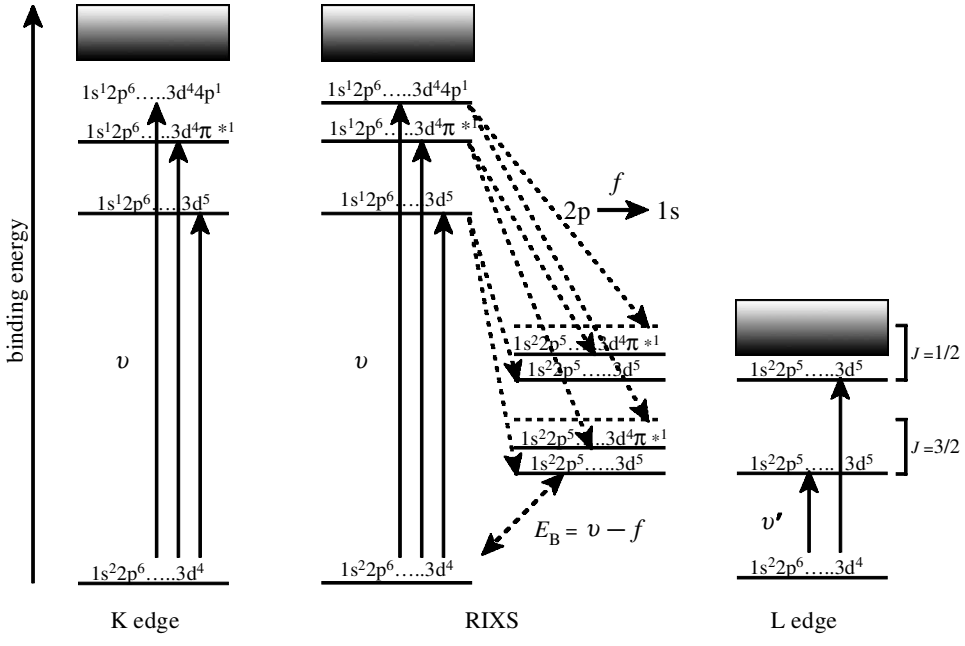

Figure 4. The electronic energy diagram of the transitions that occur in Mn K-edge, L-edge and RIXS spectroscopy. L-edge-like information is extracted from RIXS by subtracting the emission energy, *f*, from the excitation energy, υ (energy transfer, $(\upsilon - f)$ versus the incident energy, υ). However, more final states are present in the RIXS spectra than in the L-edge spectra. Therefore, RIXS gives a wealth of information about the Mn-oxidation state, ligand environment and local symmetry.

rays. Then, the high-resolution X-ray emission analyser can be tuned to detect the Kα fluorescence of Mn, which is a 2p to 1s transition. The final state from this transition is a 2p hole; the same final state as the L-edge fluorescence (3d to 2p). An advantage of RIXS over both conventional techniques is that the resonances are separated according to the final states they decay into. As a result, the resonances appear as islands in the resonant landscape and their spectral shapes can be analysed. A 2D RIXS spectrum is obtained by plotting the scanned incident X-ray energy, υ (1s to 3d), versus E_B, the binding energy, which is equal to $\upsilon - f$), *f* is the energy of the scanned high-resolution X-ray emission analyser. Furthermore, this technique offers an unprecedented opportunity to selectively excite into specific molecular orbitals with 3d character by tuning the incoming X-rays to look at a specific pre-edge transition; at least two to three resolvable pre-edge transitions are seen in the Mn K-edge spectrum of PSII. This means that it would be possible to obtain 'nested' RIXS spectra that correspond to fluorescence from different molecular orbitals with a 3d character.

We have collected preliminary data from a PSII sample in the S_1 and S_2 states. The shape and ratio of the L_{III} to L_{II}-like peaks of the PSII RIXS spectrum are in between those for the Mn^{III} and Mn^{IV} complex and very different from that for the Mn^{II} complex. This indicates a mixed (III) and (IV) Mn oxidation state in the S_1 state, i.e. (III_2,IV_2); a conclusion in accord with that derived from

other studies. The cross-sections of the 2D RIXS spectra reveal the L-edge-like character, showing two well-resolved peaks due to spin-orbit coupled states $\mathcal{J} = 3/2$ (L_{III}-like edge) and $\mathcal{J} = 1/2$ (L_{II}-like edge). The ratio of the L_{III} to L_{II} peaks increases from (II) to (III) to (IV); the ratio for PSII changes from S_1 to S_2 in a manner consistent with an oxidation from $(III)_2(IV)_2$ to $(III)(IV)_3$.

3. STRUCTURE OF THE MANGANESE CLUSTER

We have used Mn EXAFS to study the local structure of the Mn complex and have proposed topologically consistent models that can be reconciled with several structural arrangements of the four Mn atoms (DeRose *et al.* 1994). The proposed model consists of two or three di-μ-oxo-bridged binuclear Mn units with Mn–Mn distances of *ca.* 2.7 Å that are linked to each other by a mono-μ-oxo bridge with a Mn–Mn separation of *ca.* 3.3 Å, and with Ca at a distance of 3.4 Å to Mn (Yachandra *et al.* 1993; DeRose *et al.* 1994). The Mn–Mn distances are largely invariant in the native S_1 and S_2 states (DeRose *et al.* 1994). EXAFS experiments on the S_3 and S_0 states have been difficult to perform on PSII samples using single flashes. The requirement of optically dilute samples to ensure saturation by single actinic flashes generally results in a low signal-to-noise ratio. We have recently been able to extend these studies to the S_3 and S_0 states prepared by flash illumination.

(a) *S_3 state*

Earlier EXAFS data from the chemically treated S_3-state samples produced by a double turnover method indicated that the two di-μ-oxo-bridged Mn–Mn dimer units may become non-equivalent (Guiles *et al.* 1990*b*). The EXAFS spectra from Ca-depleted S_3' samples (S_2Y_Z') prepared by low pH treatment in a citrate buffer do not exhibit similar heterogeneity in 2.7 Å Mn–Mn distances (Latimer *et al.* 1998).

EXAFS data of S_3 samples created under physiological conditions with saturating flash illumination show significant changes in the Mn–Mn distances in the S_3 state compared with the S_1 and the S_2 states. The two 2.7 Å Mn–Mn distances that characterize the di-μ-oxo centres in the S_1 and S_2 states are lengthened to *ca.* 2.8 and 3.0 Å in the S_3 state, respectively (figure 5). The 3.3 Å Mn–Mn and Mn–Ca distances also increase by 0.04–0.2 Å. These changes in the Mn–Mn distances are interpreted as consequences of the onset of substrate water oxidation in the S_3 state. Mn-centred oxidation is evident during the S_0 to S_1 and S_1 to S_2 transitions. During the S_2 to S_3 transition, we propose that the changes in the Mn–Mn distances are the result of ligand or water oxidation, leading to the formation of an oxyl radical intermediate formed at a bridging or terminal position. We propose that substrate–water oxidation occurring at this transition provides the trigger for the formation of the O–O bond; the critical step in the water oxidation reaction. The reaction of the oxyl radical with OH^-, H_2O, or an oxo group during the subsequent S-state conversion is proposed to lead to the formation of the O–O bond (Liang *et al.* 2000).

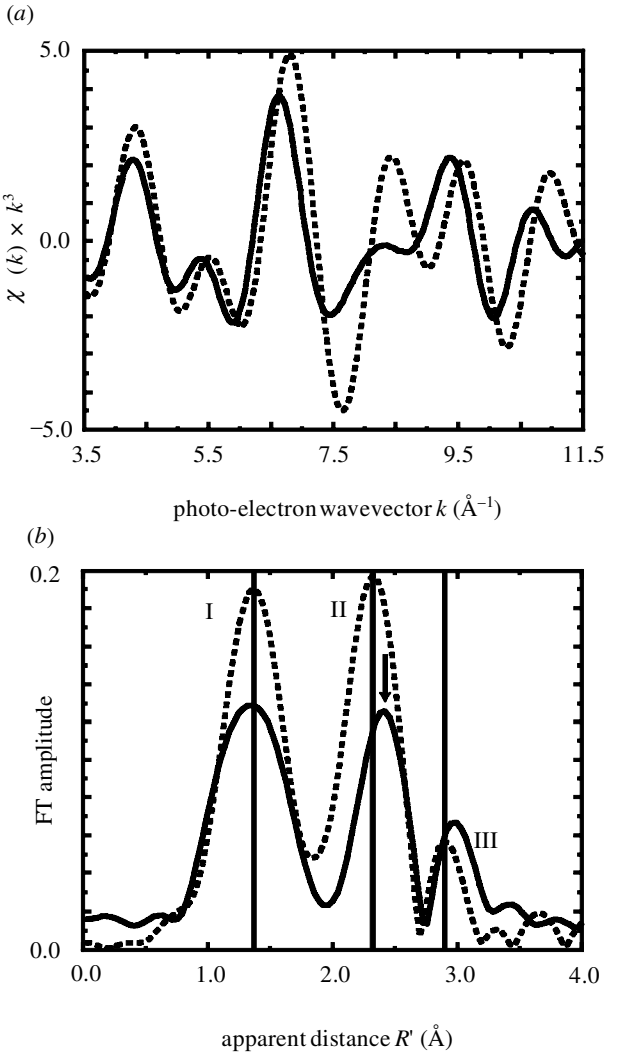

Figure 5. (*a*) Fourier-filtered *k*-space EXAFS data from S_2 (dashed line) and S_3 (solid line) state of PSII samples. The differences in phase, frequency and amplitudes between the raw S_2 and S_3 state EXAFS spectra are very obvious in these spectra. (*b*) FT power spectra of S_2 (dashed line) and S_3 (solid line) states of PSII. The major Fourier peaks are labelled I, II and III. The spectra are clearly different between the S_2 (dashed line) and S_3 states (solid line). There is a reduction in amplitude in all three peaks in the S_3 state compared with the S_2 state. More importantly, peaks II and III are at a greater apparent distance R' for the S_3 state compared with the S_2 state as shown.

(b) *S_0 state*

Although many topological structures have been proposed, on the basis of EXAFS (Penner-Hahn 1998; Dau *et al.* 2001; Robblee *et al.* 2001) and EPR (Hasegawa *et al.* 1999*a*; Peloquin & Britt 2001) studies for the Mn cluster in PSII, the issue of whether there are two or three di-μ-oxo-bridged moieties in the Mn cluster has been an open question. However, the determination of the exact number of such interactions is important for narrowing the number of options from the many that have been proposed. We have obtained data from the S_0 state that show that there may be three di-μ-oxo-bridged motifs that are characterized by the approximate 2.7 Å Mn–Mn distance.

The S_0 samples were generated by three flash illumination followed by incubation with carbonyl cyanide 4-

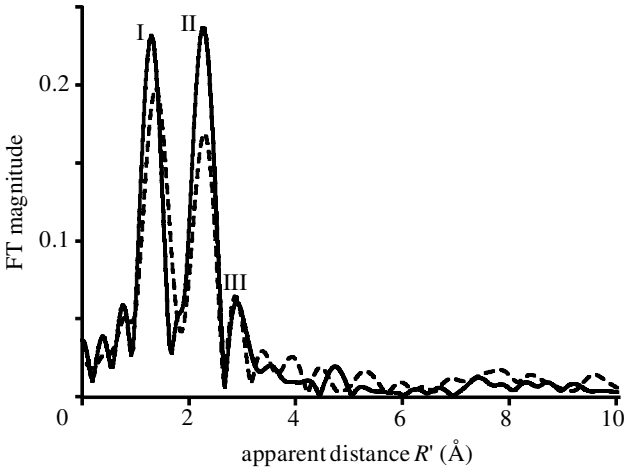

Figure 6. FTs of the S_0 (dashed line) and S_1 state (solid line) of the k^3-weighted Mn-EXAFS spectra (3.5–11.5 $Å^{-1}$). The main Fourier peaks are labelled I, II and III. There are clear differences in the amplitude and position of these peaks between the S_0 and S_1 states. The peak labelled II is from Mn–Mn interactions at *ca.* 2.7 Å.

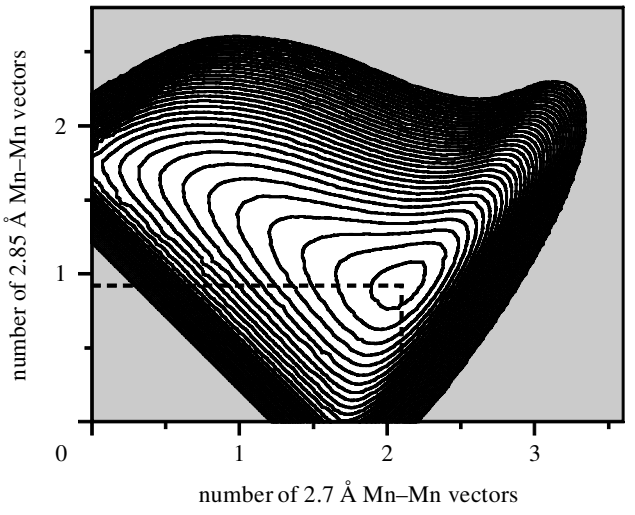

Figure 7. The contour plot shows the quality of fit parameter ε^2 for the S_0 state plotted versus the number of the two Mn–Mn interactions. The dashed lines show the distinct minimum at one Mn–Mn vector at 2.85 Å and two Mn–Mn vectors at 2.7 Å.

(trifluoromethoxy) phenyl hydrazone (Messinger *et al.* 1997*a*). The multiline EPR spectra of the S_0 and S_2 states were used to characterize all the samples.

Figure 6 shows the FTs of the k^3-weighted EXAFS data from the S_0 and S_1 states. The Fourier peak II was isolated and fit to the EXAFS equation with one or two distances for the S_0 and S_1 states. Since there has to be an integral number of Mn–Mn interactions, the fits were constrained to a ratio of 1 : 1 and 2 : 1 for the two Mn–Mn interactions. The fits for the S_1 state showed that the two distances are separated by significantly less than what can be resolved using the dataset at present. However, the situation is very different for the fits for the S_0 state. The quality of fit parameter, the ε^2 value, improved considerably on going from a one-shell to a two-shell fit, especially, in the case of the 2 : 1 ratio of Mn–Mn interactions. The result of the fitting provides evidence that there may be three short (*ca.* 2.7–2.8 Å) Mn–Mn interactions in the Mn cluster.

Figure 7 shows the best fits to two Mn–Mn distances for the S_0 state as a function of the number of each of the Mn–Mn interactions. The contour plot graphically illustrates that the global minimum at two Mn–Mn interactions at 2.7 Å and one Mn–Mn interaction at 2.85 Å is very well defined, and hence gives us confidence in its reliability. We have re-examined the data from the S_0^*, the $g = 4.1$ S_2, the NH_3- or F^--inhibited S_2 and the S_3 states, where we have shown that there is distance heterogeneity in the Mn–Mn vectors. In each case, the ratio of the number of the two Mn–Mn interactions was *ca.* 2 : 1. This leads us to think that there may be three Mn interactions at *ca.* 2.7 Å in the Mn cluster in its native state, one of which is perturbed in the S_0, F^-- and NH_3-inhibited S_2 and the $g = 4.1$ S_2 states, and all three are perturbed in the S_3 state.

We showed earlier that there are several topological models that are compatible with our EXAFS data. These models have been described in detail (DeRose *et al.* 1994; Robblee *et al.* 2001). However, only one of those options (A) is widely used as a working model, although options E, F and G (the nomenclature is from DeRose *et al.* (1994)) have been shown to be preferred on the basis of EPR and electron nuclear double resonance simulations (Hasegawa *et al.* 1999*b*; Peloquin & Britt 2001). On the basis of the present results from the S_0 state, we think it is important to consider the options that include three di-μ-oxo-bridged moieties in the Mn cluster. Figure 8 shows several such options, G, I and J, that were proposed earlier, and two newer options, L and M, among several others that can be conceived. Options J and I are less probable structures because J lacks a Mn–Mn interaction at 3.3 Å, and I has two such interactions. The EXAFS data from an inorganic compound (Auger *et al.* 1990) with the motif in option J are very different from those obtained from a PSII sample (R. M. Cinco and V. K. Yachandra, unpublished data). Options G, L and M all have three di-μ-oxo bridges and one mono-μ-oxo bridge; that is three 2.7 Å Mn–Mn interactions and one 3.3 Å Mn–Mn interaction and are qualitatively in agreement with the asymmetry seen in the electron density of the Mn cluster (Zouni *et al.* 2001). Options L and M are also similar to the structure proposed on the basis of density functional theory calculations (Siegbahn 2000). We are in the process of testing the compatibility of various Mn models that satisfy the criteria set by the distance data and orientation of the various Mn–Mn, Mn–Ca vectors obtained from EXAFS with the electron-density data obtained from X-ray crystallography.

4. THE ROLE OF THE CALCIUM COFACTOR

Calcium and chloride are the necessary cofactors for the proper function of the OEC of PSII (Debus 1992). While the Mn complex has been extensively studied by X-ray absorption techniques (XANES and EXAFS) comparatively less is known about the Ca^{2+} cofactor. The fewer number of studies on the Ca^{2+} cofactor have sometimes relied on substituting the native cofactor with Sr or other metals (Ghanotakis *et al.* 1985; Boussac & Rutherford 1988) and have stirred some debate about the structure

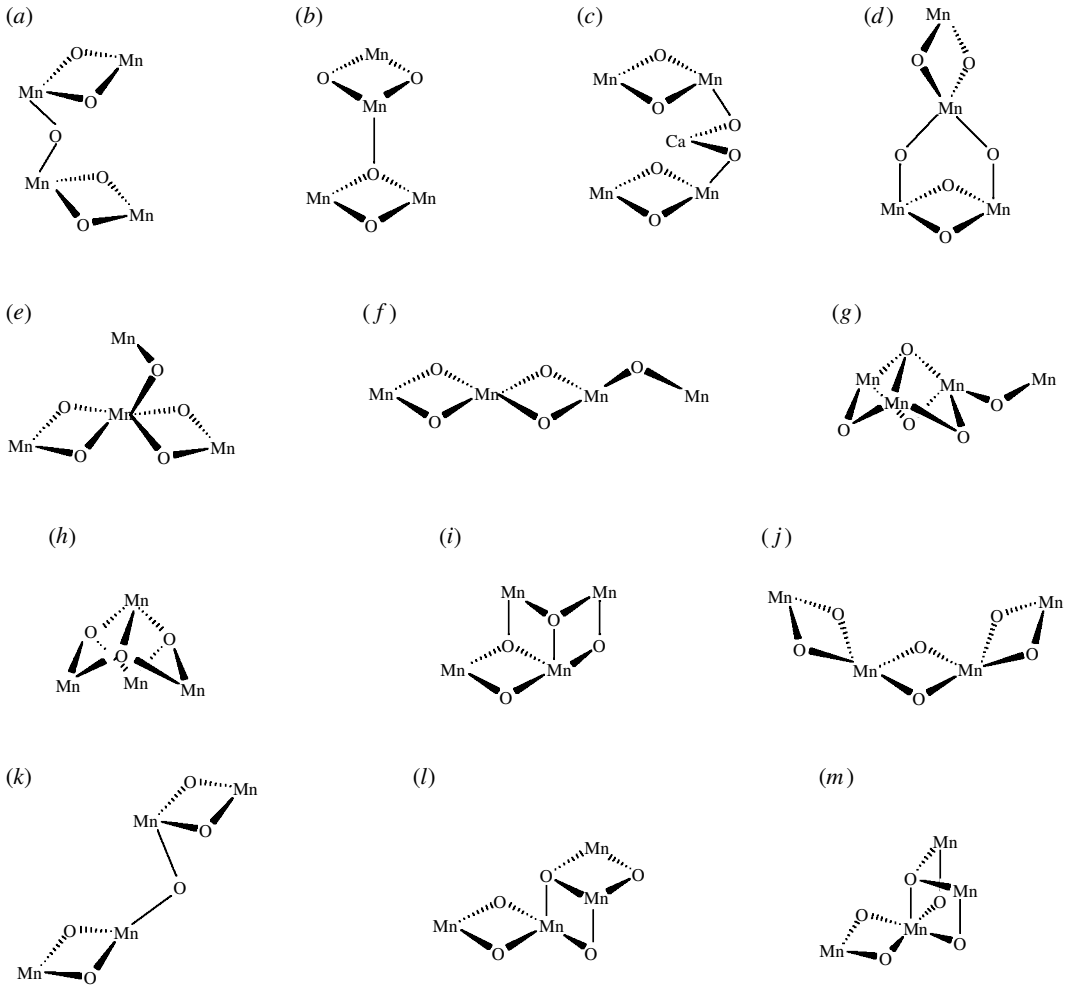

Figure 8. Structural models for the Mn cluster with three di-μ-oxo-bridged Mn moieties. Options G, I, and J are from DeRose *et al.* (1994), and L and M are two other viable options. One or two mono-μ-oxo-bridged motifs are also present in options G, I, L and M. No such motif exists in option J.

of the binding site. Past efforts using Mn EXAFS on Sr-substituted PSII have indicated a close link between the Mn cluster and Sr, within 3.5 Å (Latimer *et al.* 1995). The most recently published study using Sr EXAFS on similar samples confirms this finding of a 3.5 Å distance between Mn and Sr (Cinco *et al.* 1998). This finding was based on a second Fourier peak in the Sr EXAFS from functional samples, but is absent from inactive, hydroxylamine-treated PSII. This Fourier peak II was found to fit best to two Mn at 3.5 Å rather than lighter atoms (carbon). Nevertheless, other experiments have given contrasting results (RiggsGelasco *et al.* 1996).

(a) *Orientated strontium extended X-ray absorption fine structure*

We have extended the technique using polarized Sr EXAFS on layered Sr-substituted samples to provide important angle information. Polarized EXAFS involves collecting spectra for different incident angles (θ) between the membrane normal of the layered sample and the X-ray electric field vector. Dichroism in the EXAFS can occur, depending on how the particular absorber–backscatterer (A–B) vector is aligned with the electric field. Through analysis of the dichroism, we extract the average orientation (ϕ) of this A–B vector relative to the membrane normal and the average number of scatters per absorbing atom (N_{iso}). Constraints on the structural model are then imposed by these parameters.

Sr-substituted PSII samples were made by a process of Ca^{2+} depletion Sr^{2+} reactivation and Chelex treatment to remove any excess Sr^{2+} (Cinco *et al.* 1998). Orientated samples were made by layering onto flat Mylar films (Mukerji *et al.* 1994; Dau *et al.* 1995). The FTs from the polarized Sr EXAFS showed extreme dichroism in Fourier peak II (figure 9). Preliminary nonlinear least-squares regression analysis produced the solid curve shown in figure 9 as the best fit of the 15 data points (angles from six separate samples) and the result translates to 1–2 Sr–Mn vectors with an average angle of $23 \pm 4°$ from the membrane normal.

The orientation data from the Sr EXAFS experiments can be combined with the dichroism data from Mn EXAFS data to calculate the orientation of the 3.3 Å Mn–Mn vector. Fourier peak III in the Mn EXAFS, which contains Mn–Mn (3.3 Å) and Mn–Ca (3.4 Å) contributions, is dichroic, with an average angle of $43 \pm 10°$ with respect to the membrane normal (Mukerji *et al.* 1994). By including the Mn–Ca vector at 23°, we calculate an angle of *ca.* 62° for the 3.3 Å Mn–Mn vector. Previous polarized Mn EXAFS experiments on PSII have shown angles of 55° and 67° for the 2.7 Å Mn–Mn vectors (Mukerji *et al.* 1994; Dau *et al.* 1995). All Mn–Mn vectors then lie at

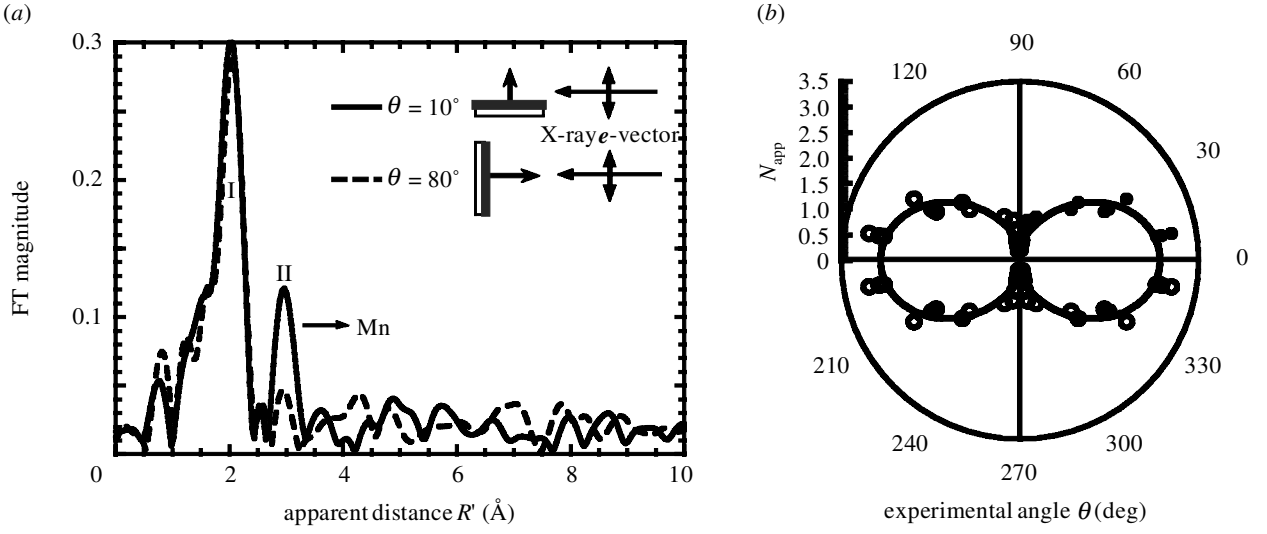

Figure 9. (*a*) FTs of k^3-weighted Sr EXAFS from orientated Sr–PSII; samples at two angles (θ). The dichroism is most readily apparent in Fourier peak II ($R' = 3.0$ Å) which is assigned to backscattering from Mn. (*b*) The polar plot shows N_{exp} (black circles) plotted versus the angle of detection, θ. The solid line is the best fit from which we obtain N_{iso} (number of Mn neighbours to Sr) and ϕ, the angle the Mn–Sr vector makes with the membrane normal.

roughly the same angle (*ca.* 60°) with respect to the membrane plane, but are not restricted to being collinear, because the PSII membranes are ordered in one dimension only.

(b) *Calcium extended X-ray absorption fine structure*

In a complementary and definitive experiment, we have used Ca K-edge EXAFS studies to probe the binding site of the native cofactor for any nearby Mn, within *ca.* 4 Å. This is analogous to the Sr EXAFS studies already published (Cinco *et al.* 1998), but it focuses on the native cofactor and avoids the treatments involving Ca depletion and Sr substitution. This technique is a more sensitive and direct probe of the Ca binding site in PSII than Sr EXAFS.

Chelex-treated PSII (2 Ca per 4 Mn per PSII) was accumulated on the flat surface of solid Plexiglas (Ca free) while not affecting oxygen-evolving activity or the S_2 EPR multiline signal. To prepare the parallel control (inactive) sample, 40 μl of hydroxylamine (NH_2OH, 100 mM) was added to the surface of the layered PSII and was allowed to soak and dry without loss of PSII material.

The FT of the Ca EXAFS is presented in figure 10. The spectra are remarkably similar to the Fourier transforms of the earlier Sr EXAFS study with Sr substituted for Ca. The first (largest) Fourier peak corresponds to the coordinating oxygen atoms closest to Ca. In contrast to the control (NH_2OH-treated) sample, the Chelex-treated PSII shows a second Fourier peak. When this peak II is isolated and simulated with possible scattering atoms, it corresponded best to Mn at 3.4 Å, rather than to light atom (C, O or Cl) neighbours. These results were consistent with the earlier Sr EXAFS studies (Cinco *et al.* 1998).

The Ca EXAFS protocol has directly probed the Ca cofactor in its native state, avoiding potentially disruptive treatments such as the low pH exposure involved in metal substitution. This result provides proof of the Mn–Ca heteronuclear cluster as the catalytic site of oxygen evolution in PSII.

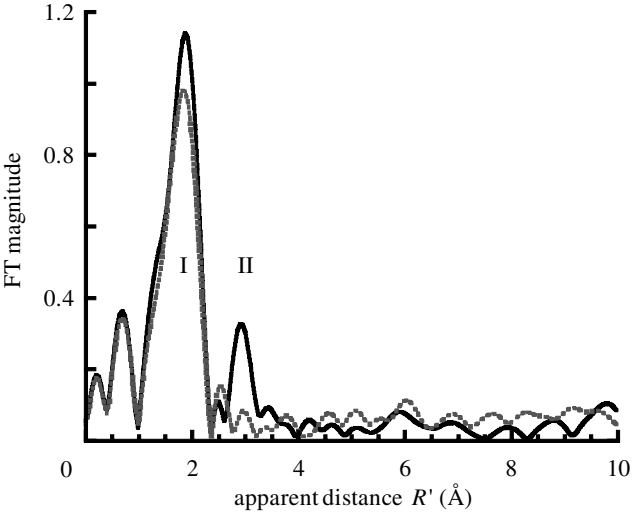

Figure 10. FT of Ca EXAFS from Chelex-treated, layered samples with 2 Ca per PSII (k^3 weighted, $k = 2.5$–10.5 Å^{-1}. The FTs show the presence of a second Fourier peak in the 2 Ca per PSII sample that fits to Ca–Mn that is absent in the control sample. Solid line, intact 2 Ca per PSII (Chelex treated); dashed line, inactive 2 Ca per PSII (NH_2OH treated).

Due to the fact that significant angle information about Mn–Mn and Mn–Ca vectors is now available as described above, other topological models previously discussed (DeRose *et al.* 1994) can be refined to include the presence of Ca and account for the dichroism data. Three possible refined models are presented in figure 11. Recent EXAFS data from the S_0 state has indicated that there may be three di-μ-oxo-bridged Mn–Mn units (see above). However, such motifs were not included in figure 11, but considering them is a subject for future work.

5. MECHANISM OF WATER OXIDATION

The many mechanisms of water oxidation that have been proposed can be broadly divided into four groups,

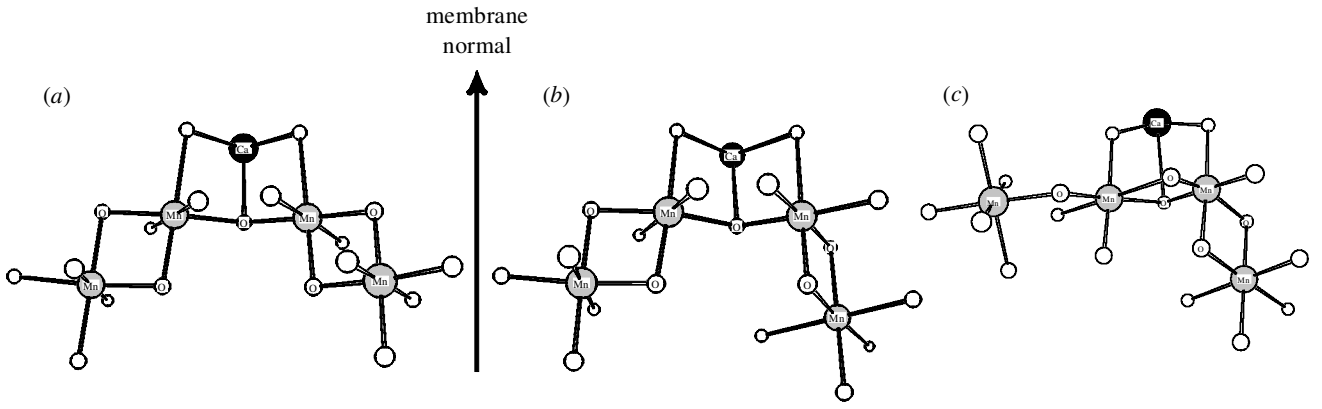

Figure 11. Refined models for the active site of the OEC in PSII. These models combine the finding from orientated Sr-substituted PSII samples with previous results from Mn EXAFS on orientated PSII samples. These are derived from core structures that have been described in earlier studies ((*a*) and (*b*) from option A and (*c*) from option F in DeRose *et al.* (1994)). Mn and Ca atoms are as labelled and the white circles with those with circles in represent oxygen atoms.

in which the kind of oxygen atom (Mn-terminal oxygen ligand, Mn-bridging oxygen ligand or exogenous oxygen from water or hydroxide) involved in O–O bond formation is different. In these four groups the oxygen atoms can de derived from two terminal oxygen atoms bound to Mn atoms (Haumann & Junge 1999; Hoganson & Babcock 2000; Limburg *et al.* 2000; Messinger *et al.* 2001; Renger 2001; Robblee *et al.* 2001; Hillier & Wydrzynski 2001), one bridging or terminal oxygen and one exogenous oxygen (Siegbahn & Crabtree 1999; Dau *et al.* 2001; Hillier & Wydrzynski 2001; Kuzek & Pace 2001; Messinger *et al.* 2001; Robblee *et al.* 2001; Vrettos *et al.* 2001), one terminal and one bridging oxygen (Limburg *et al.* 2000; Nugent *et al.* 2001) or two bridging oxygens (Brudvig & Crabtree 1986; Christou & Vincent 1987; Messinger *et al.* 2001; Robblee *et al.* 2001). The results that have a direct bearing on this subject are the $H_2{}^{16}O$–$H_2{}^{18}O$ exchange studies by Messinger and co-workers that support the presence of two non-equivalent exchangeable sites in the S_3 state (Messinger *et al.* 1995; Hillier *et al.* 1998).

We have proposed earlier a model for the S_3 state in which an oxyl radical is generated on one of the μ-oxo bridges, that results in an increase of one of the Mn–Mn distances to *ca*. 2.95 Å (figure 5) (Yachandra *et al.* 1996; Liang *et al.* 2000). Consistent with our XANES results is the implication in this structure that the oxidative equivalent is not stored on the Mn atoms *per se* during the $S_2 \rightarrow S_3$ transition but is delocalized with significant charge and spin density on the bridging oxo ligand. These data are reinforced by our Mn Kβ emission studies of the various S states (Messinger *et al.* 2001). Second, the Mn–Mn distance in both of the di-μ-oxo-bridged units increases from 2.72 to 2.82 Å and 2.95 Å upon the formation of the S_3 state. These changes imply a significant structural change in the Mn cluster as it proceeds to the S_3 state. It is difficult to rationalize such changes in Mn–Mn distance as arising purely from Mn oxidation or involving Mn terminal ligands. It is difficult to understand how changes in terminal ligation can generate such a profound change on the Mn–Mn distances in the S_3 state. Replacement of terminal ligands in di-μ-oxo-bridged model compounds has a minimal effect on the Mn–Mn distance of 2.7 Å that is characteristic of such di-μ-oxo-bridged Mn compounds (Wieghardt 1989; Pecoraro 1992). However, it is easier to rationalize increases in Mn–Mn distances as being due to changes in the bridging structure. We propose that substrate–water oxidation chemistry is occurring at the S_2 to S_3 transition as evidenced by the lack of Mn oxidation, and leading to the significant structural changes as seen in the increase in the Mn–Mn distances. Our proposed mechanism, where the O–O bond is formed between one critical bridging oxygen and another oxygen atom derived from a bridging or terminal oxygen ligand or an exogenous oxygen also avoids the formation of the O–O bond until the most oxidized state (S_4) is reached. This precludes the formation and release of peroxide or other oxidation products of water in the earlier S states, thus preventing the system from 'short circuiting' and avoiding the risk of damaging the polypeptides of PSII.

This work was supported by a National Institutes of Health grant (GM 55302) and by the Director, Office of Science, Office of Basic Energy Sciences, Division of Energy Biosciences, US Department of Energy under contract no. DE-AC03-76SF00098. The important contributions to the research presented in this article by Dr R. Cinco, Dr J. Robblee, Dr J. Messinger, Dr H. Visser, Dr U. Bergmann, Dr P. Glatzel, Dr C. Fernandez, Dr E. Anxolabéhère-Mallart, Dr S. Pizarro, Dr K. McFarlane, Dr J. Yano, Professor M. Klein, Professor K. Sauer and Professor S. Cramer are gratefully acknowledged. The author thanks his collaborators, Professor W. H. Armstrong, Professor G. Christou, Professor J.-J. Girerd, Professor R. N. Mukherjee and Professor K. Wieghardt for providing all the inorganic Mn compounds. Synchrotron radiation facilities were provided by the Stanford Synchrotron Radiation Laboratory (SSRL) and the Advanced Photon Source (APS), both supported by the US Department of Energy. The Biotechnology Laboratory at SSRL and BioCAT at the APS are supported by the National Center for Research Resources of the National Institutes of Health.

REFERENCES

Ahrling, K. A., Peterson, S. & Styring, S. 1997 An oscillating manganese electron paramagnetic resonance signal from the S_0 state of the oxygen evolving complex in photosystem II. *Biochemistry* **36**, 13 148–13 152.

Auger, N., Girerd, J.-J., Corbella, M., Gleizes, A. & Zimmermann, J.-L. 1990 Synthesis, structure, and magnetic properties of the stable triangular $[Mn(IV)_3O_4]^{4+}$ core. *J. Am. Chem. Soc.* **112**, 448–450.

Bergmann, U. & Cramer, S. P. 1998 A high-resolution large-acceptance analyzer for x-ray fluorescence and Raman spectroscopy. In *Proc. SPIE, Crystal and Multilayer Optics*, vol. 3448, pp. 198–210. San Diego, CA: SPIE.

Boussac, A. & Rutherford, A. W. 1988 Nature of the inhibition of the oxygen-evolving enzyme of photosystem-II induced by NaCl washing and reversed by the addition of Ca^{2+} or Sr^{2+}. *Biochemistry* **27**, 3476–3483.

Brudvig, G. W. & Crabtree, R. H. 1986 Mechanism for photosynthetic oxygen evolution. *Proc. Natl Acad. Sci. USA* **83**, 4586–4588.

Caliebe, W. A., Kao, C.-C., Hastings, J. B., Taguchi, M., Kotani, A., Uozumi, T. & DeGroot, F. M. F. 1998 1s2p resonant inelastic x-ray scattering in α-FeO_3. *Phys. Rev.* B **58**, 13 542–13 548.

Christou, G. & Vincent, J. B. 1987 The molecular double-pivot mechanism for water oxidation. *Biochim. Biophys. Acta* **895**, 259–274.

Cinco, R. M., Robblee, J. H., Rompel, A., Fernandez, C., Yachandra, V. K., Sauer, K. & Klein, M. P. 1998 Strontium EXAFS reveals the proximity of calcium to the manganese cluster of oxygen-evolving photosystem II. *J. Phys. Chem.* B **102**, 8248–8256.

Dau, H., Andrews, J. C., Roelofs, T. A., Latimer, M. J., Liang, W. C., Yachandra, V. K., Sauer, K. & Klein, M. P. 1995 Structural consequences of ammonia binding to the manganese center of the photosynthetic oxygen-evolving complex—an X-ray-absorption spectroscopy study of isotropic and oriented photosystem-II particles. *Biochemistry* **34**, 5274–5287.

Dau, H., Iuzzolino, L. & Dittmer, J. 2001 The tetra-manganese complex of photosystem II during its redox cycle—X-ray absorption results and mechanistic implications. *Biochim. Biophys. Acta* **1503**, 24–39.

Debus, R. J. 1992 The manganese and calcium-ions of photosynthetic oxygen evolution. *Biochim. Biophys. Acta* **1102**, 269–352.

Dekker, J. P. 1992 Optical studies on the oxygen-evolving complex of photosystem II. In *Manganese redox enzymes* (ed. V. L. Pecoraro), pp. 85–103. New York: VCH.

DeRose, V. J., Mukerji, I., Latimer, M. J., Yachandra, V. K., Sauer, K. & Klein, M. P. 1994 Comparison of the manganese oxygen-evolving complex in photosystem II of spinach and *Synechococcus* sp. with multinuclear manganese model compounds by X-ray absorption spectroscopy. *J. Am. Chem. Soc.* **116**, 5239–5249.

Dismukes, G. C. & Siderer, Y. 1981 Intermediates of a polynuclear manganese center involved in photosynthetic oxidation of water. *Proc. Natl Acad. Sci. USA* **78**, 274–278.

Ghanotakis, D. F., Babcock, G. T. & Yocum, C. F. 1985 Structure of the oxygen-evolving complex of photosystem II: calcium and lanthanum compete for sites on the oxidizing side of photosystem II which control the binding of water-soluble polypeptides and regulate the activity of the manganese complex. *Biochim. Biophys. Acta* **809**, 173–180.

Guiles, R. D., Yachandra, V. K., McDermott, A. E., Cole, J. L., Dexheimer, S. L., Britt, R. D., Sauer, K. & Klein, M. P. 1990*a* The S_0 state of photosystem-II induced by hydroxylamine—differences between the structure of the manganese complex in the S_0 and S_1 states determined by X-ray absorption-spectroscopy. *Biochemistry* **29**, 486–496.

Guiles, R. D. (and 10 others) 1990*b* The S_3 state of photosystem II: differences between the structure of the manganese complex in the S_2 and S_3 states determined by X-ray absorption spectroscopy. *Biochemistry* **29**, 471–485.

Hansson, Ö. & Andréasson, L.-E. 1982 EPR-detectable magnetically interacting manganese ions in the photosynthetic oxygen-evolving system after continuous illumination. *Biochim. Biophys. Acta* **679**, 261–268.

Hasegawa, K., Ono, T.-A., Inoue, Y. & Kusunoki, M. 1999*a* How to evaluate the structure of a tetranuclear Mn cluster from magnetic and EXAFS data: case of the S_2-state Mn-cluster in photosystem II. *Bull. Chem. Soc. Jpn.* **72**, 1013–1023.

Hasegawa, K., Ono, T.-A., Inoue, Y. & Kusunoki, M. 1999*b* Spin-exchange interactions in the S_2-state manganese tetramer in photosynthetic oxygen-evolving complex deduced from g=2 multiline EPR signal. *Chem. Phys. Lett* **300**, 9–19.

Haumann, M. & Junge, W. 1999 Photosynthetic water oxidation: a simplex-scheme of its partial reactions. *Biochim. Biophys. Acta* **1411**, 86–91.

Hillier, W. & Wydrzynski, T. 2001 Oxygen ligand exchange at metal sites—implications for the O_2 evolving mechanism of photosystem II. *Biochim. Biophys. Acta* **1503**, 197–209.

Hillier, W., Messinger, J. & Wydrzynski, T. 1998 Kinetic determination of the fast exchanging substrate water molecule in the S_3 state of photosystem II. *Biochemistry* **37**, 16 908–16 914.

Hoganson, C. W. & Babcock, G. T. 2000 Mechanistic aspects of the tyrosyl radical-manganese complex in photosynthetic water oxidation. In *Manganese and its role in biological processes*, vol. 37 (ed. A. Sigel & H. Sigel), pp. 613–656. New York: Marcel Dekker.

Iuzzolino, L., Dittmer, J., Dörner, W., Meyer-Klaucke, W. & Dau, H. 1998 X-ray absorption spectroscopy on layered photosystem II membrane particles suggests manganese-centered oxidation of the oxygen-evolving complex for the S_0–S_1, S_1–S_2 and S_2–S_3 transitions of the water oxidation cycle. *Biochemistry* **37**, 17 112–17 119.

Kok, B., Forbush, B. & McGloin, M. 1970 Cooperation of charges in photosynthetic oxygen evolution. I. A linear four step mechanism. *Photochem. Photobiol.* **11**, 457–475.

Kuzek, D. & Pace, R. J. 2001 Probing the Mn oxidation states in the OEC. Insights from spectroscopic, computational and kinetic data. *Biochim. Biophys. Acta* **1503**, 123–137.

Latimer, M. J., DeRose, V. J., Mukerji, I., Yachandra, V. K., Sauer, K. & Klein, M. P. 1995 Evidence for the proximity of calcium to the manganese cluster of photosystem II—determination by X-ray-absorption spectroscopy. *Biochemistry* **34**, 10 898–10 909.

Latimer, M. J., DeRose, V. J., Yachandra, V. K., Sauer, K. & Klein, M. P. 1998 Structural effects of calcium depletion on the manganese cluster of photosystem II: determination by X-ray absorption spectroscopy. *J. Phys. Chem.* B **102**, 8257–8265.

Liang, W., Roelofs, T. A., Cinco, R. M., Rompel, A., Latimer, M. J., Yu, W. O., Sauer, K., Klein, M. P. & Yachandra, V. K. 2000 Structural change of the Mn cluster during the S2 → S3 state transition of the oxygen-evolving complex of photosystem II. Does it reflect the onset of water/substrate oxidation? Determination by Mn X-ray absorption spectroscopy. *J. Am. Chem. Soc.* **122**, 3399–3412.

Limburg, J., Brudvig, G. W. & Crabtree, R. H. 2000 Modeling the oxygen-evolving complex in photosystem II. In *Biomimetic oxidations catalyzed by transition metal complexes* (ed. B. Meunier), pp. 509–541. London: Imperial College.

Messinger, J., Badger, M. & Wydrzynski, T. 1995 Detection of one slowly exchanging substrate water molecule in the S_3 state of photosystem-II. *Proc. Natl Acad. Sci. USA* **92**, 3209–3213.

Messinger, J., Nugent, J. H. A. & Evans, M. C. W. 1997*a* Detection of an EPR multiline signal for the S_0 state in photosystem II. *Biochemistry* **36**, 11 055–11 060.

Messinger, J., Robblee, J. H., Yu, W. O., Sauer, K., Yachandra, V. K. & Klein, M. P. 1997*b* The S_0 state of the oxygen-evolving complex in photosystem II is paramagnetic: detec-

tion of an EPR multiline signal. *J. Am. Chem. Soc.* **119**, 11 349–11 350.
Messinger, J. (and 13 others) 2001 Absence of Mn-centered oxidation in the S_2 to S_3 transition: implications for the mechanism of photosynthetic water oxidation. *J. Am. Chem. Soc.* **123**, 7804–7820.
Mukerji, I., Andrews, J. C., Derose, V. J., Latimer, M. J., Yachandra, V. K., Sauer, K. & Klein, M. P. 1994 Orientation of the oxygen-evolving manganese complex in a photosystem-II membrane preparation—an X-ray-absorption spectroscopy study. *Biochemistry* **33**, 9712–9721.
Nugent, J. H. A., Rich, P. & Evans, M. C. W. 2001 Photosynthetic water oxidation: towards a mechanism. *Biochim. Biophys. Acta* **1503**, 138–146.
Ono, T., Noguchi, T., Inoue, Y., Kusunoki, M., Matsushita, T. & Oyanagi, H. 1992 X-ray-detection of the period-4 cycling of the manganese cluster in photosynthetic water oxidizing enzyme. *Science* **258**, 1335–1337.
Pecoraro, V. L. 1992 *Manganese redox enzymes*. New York: VCH Publishers.
Peloquin, J. M. & Britt, R. D. 2001 EPR/ENDOR characterization of the physical and electronic structure of the OEC Mn cluster. *Biochim. Biophys. Acta* **1503**, 96–111.
Peng, G. (and 10 others) 1994 High-resolution manganese X-ray-fluorescence spectroscopy—oxidation-state and spin-state sensitivity. *J. Am. Chem. Soc.* **116**, 2914–2920.
Penner-Hahn, J. E. 1998 Structural characterization of the Mn site in the photosynthetic oxygen-evolving complex. *Struct. Bond. (Berlin)* **90**, 1–36.
Renger, G. 2001 Photosynthetic water oxidation to molecular oxygen: apparatus and mechanism. *Biochim. Biophys. Acta* **1503**, 210–228.
RiggsGelasco, P. J., Mei, R., Ghanotakis, D. F., Yocum, C. F. & PennerHahn, J. E. 1996 X-ray absorption spectroscopy of calcium-substituted derivatives of the oxygen-evolving complex of photosystem II. *J. Am. Chem. Soc.* **118**, 2400–2410.
Robblee, J. H., Cinco, R. M. & Yachandra, V. K. 2001 X-ray spectroscopy-based structure of the Mn cluster and mechanism of photosynthetic oxygen evolution. *Biochim. Biophys. Acta* **1503**, 7–23.
Roelofs, T. A., Liang, M. C., Latimer, M. J., Cinco, R. M., Rompel, A., Andrews, J. C., Sauer, K., Yachandra, V. K. & Klein, M. P. 1996 Oxidation states of the manganese cluster during the flash-induced S-state cycle of the photosynthetic oxygen-evolving complex. *Proc. Natl Acad. Sci. USA* **93**, 3335–3340.
Sharp, R. R. 1992 Proton NMR relaxation due to the photosynthetic oxygen-evolving center. In *Manganese redox enzymes* (ed. V. L. Pecoraro), pp. 177–196. New York: VCH.
Siegbahn, P. E. M. 2000 Theoretical models for the oxygen radical mechanism of water oxidation and of the water oxidizing complex of photosystem II. *Inorganic Chem.* **39**, 2923–2935.
Siegbahn, P. E. M. & Crabtree, R. H. 1999 Manganese oxyl radical intermediates and O–O bond formation in photosynthetic oxygen evolution and a proposed role for the calcium cofactor in photosystem II. *J. Am. Chem. Soc.* **121**, 117–127.
Styring, S. A. & Rutherford, A. W. 1988 The microwave-power saturation of SII_{slow} varies with the redox state of the oxygen-evolving complex in photosystem-II. *Biochemistry* **27**, 4915–4923.
Van Leeuwen, P. J., Heimann, C. & Vangorkom, H. J. 1993 Absorbency difference spectra of the S-state transitions in photosystem-II core particles. *Photosynth. Res.* **38**, 323–330.
Visser, H., Anxolabéhère-Mallart, E., Bergman, U., Glatzel, P., Robblee, J. H., Cramer, S. P., Girerd, J.-J., Sauer, K., Klein, M. P. & Yachandra, V. K. 2001 Mn K-edge XANES and Kβ XES studies of two Mn-oxo binuclear complexes. Investigation of three different oxidation states relevant to the oxygen-evolving complex of photosystem II. *J. Am. Chem. Soc.* **123**, 7031–7039.
Vrettos, J. S., Limburg, J. & Brudvig, G. W. 2001 Mechanism of photosynthetic water oxidation: combining biophysical studies of photosystem II with inorganic model chemistry. *Biochim. Biophys. Acta* **1503**, 229–245.
Wang, H., Peng, G., Miller, L. M., Scheuring, E. M., George, S. J., Chance, M. R. & Cramer, S. P. 1997 Iron L-edge X-ray absorption spectroscopy of myoglobin complexes and photolysis products. *J. Am. Chem. Soc.* **119**, 4921–4928.
Wang, X., de Groot, F. & Cramer, S. P. 1996 X-ray magnetic circular dichroism spectra and distortions at Fe^{2+} $L_{2,3}$ edges. *J. Electron Spectrosc. Relat. Phenom.* **78**, 337–340.
Wieghardt, K. 1989 The active-sites in manganese-containing metalloproteins and inorganic model complexes. *Angew. Chem. Int. Ed. English* **28**, 1153–1172.
Yachandra, V. K. 1995 X-ray absorption spectroscopy and applications in structural biology. In *Methods in enzymology*, vol. 246 (ed. K. Sauer), pp. 638–675. Orlando, FL: Academic.
Yachandra, V. K. & Klein, M. P. 1996 X-ray absorption spectroscopy: determination of transition metal site structures in photosynthesis. *Adv. Photosynth.* **3**, 337–354.
Yachandra, V. K., Derose, V. J., Latimer, M. J., Mukerji, I., Sauer, K. & Klein, M. P. 1993 Where plants make oxygen—a structural model for the photosynthetic oxygen-evolving manganese cluster. *Science* **260**, 675–679.
Yachandra, V. K., Sauer, K. & Klein, M. P. 1996 Manganese cluster in photosynthesis: where plants oxidize water to dioxygen. *Chem. Rev.* **96**, 2927–2950.
Zouni, A., Witt, H. T., Kern, J., Fromme, P., Krauss, N., Saenger, W. & Orth, P. 2001 Crystal structure of photosystem II from *Synechococcus elongatus* at 3.8 angstrom resolution. *Nature* **409**, 739–743.

Discussion

W. Junge (*Abteilung Biophysik, Universität Osnabrück, Osnabrück, Germany*). Is there any evidence for the involvement of Mn^V in the S-state cycle?

V. K. Yachandra. We have not detected any Mn^V in the S_0 through to the S_3 state. Mn^V has a distinctive pre-edge feature in the Mn XANES and if it was present, it would be quite easy to detect.

C. Dismukes (*Department of Chemistry, Princeton University, Princeton, NJ, USA*). Since there is a large structural change in the S_2 to S_3 transitions (as evident in your EXAFS data) would that not also result in a substantial change in the XANES K-edge data that would obscure the sharp edge seen in the other S-state changes? In other words, how can you conclude that there is no Mn oxidation on the S_2 to S_3 transition based on the absence of a sharp edge shift?

V. K. Yachandra. There is a lengthening of the Mn–Mn distance from 2.7 Å in the S_2 state to *ca.* 2.82 and *ca.* 2.95 Å in the S_3 state. In three Mn model compounds in similar oxidation states, investigated by Vince Pecoraro and Jim Penner-Hahn, where the Mn–Mn distance changes from 2.7 to 2.8 or to 2.9 Å, the Mn K-edge is at the same energy position in all three cases. However, if you are looking at complexes with completely different structures then it is possible that the oxidation state correlation with K-edge inflection point energy could be complicated. However, to address such questions precisely, we carried out Mn Kβ emission studies. As I showed in my

talk using model compounds, the Kβ emission spectra are influenced very little by structural change and are predominantly dependent on the oxidation state of Mn. So the combination of Mn K-edge XANES and Kβ emission studies of PSII in all the S-states leads us to conclude that there is no Mn-centred oxidation in the S_2 to S_3 transition.

L. Hammarström (*Department of Physical Chemistry, Uppsala University, Uppsala, Sweden*). Longer distances in the S_0 state are consistent with either Mn^{II} or Mn^{III}. But you have indicated that two Mn–Mn distances become longer in the S_2 to S_3 transition. If you put a radical on one oxygen then would you expect Mn–Mn distance changes in more than one of the binuclear Mn units?

V. K. Yachandra. Your question raises an important point—how can we account for the increase in two Mn–Mn distances if the radical is formed on only one di-μ-oxo-bridged unit. The oxidation of the bridging oxo group provides an explanation for an increase in distance of one di-μ-oxo-bridged Mn–Mn moiety from 2.7 Å in the S_2 state to *ca*. 3.0 Å in the S_3 state. But it is difficult to understand why, in model A, the other di-μ-oxo Mn–Mn moiety also increased in distance even though it was somewhat isolated from the proposed oxyl radical. Thus, it would be more logical if the structure of the OEC was in fact more 'tied together' than that shown in A, which would more easily explain the lengthening of all di-μ-oxo Mn–Mn motifs in the S_3 state. From the topological models, model G seems best suited to understand the structural changes during the S_2 to S_3 transition. If G is used, formation of an oxyl radical at one of the di-μ-oxo bridges for example, would give rise to the longer *ca*. 3.0 Å Mn–Mn distance in the S_3 state. The lengthening of the other di-μ-oxo Mn–Mn moieties can be explained if some of the spin density of the oxyl radical in G is present on the μ_3-oxo bridge or the other μ_2-oxo bridges. Similarly, for structures L and M, one of the di-μ-oxo-bridged oxygen becomes the oxyl radical and gives rise to the 3.0 Å Mn–Mn distance in the S_3 state. In a manner similar to what was proposed above for G, the increase in the other Mn–Mn distances can be rationalized by some of this spin density being present on the μ_3-oxo-bridged oxygen or the other μ_2-oxo-bridged oxygens.

GLOSSARY

EPR: electron paramagnetic resonance
EXAFS: extended X-ray absorption fine structure
FT: Fourier transform
OEC: oxygen-evolving complex
PSII: photosystem II
RIXS: resonant inelastic X-ray scattering spectroscopy
XANES: X-ray absorption near-edge structure
XES: X-ray emission spectroscopy